Published in final edited form as:
Cell Metab. 2014 September 2; 20(3): 471–482. doi:10.1016/j.cmet.2014.06.002.

Xbp1s in Pomc neurons connects ER stress with energy balance and glucose homeostasis

Kevin W. Williams[1,4,14,*], **Tiemin Liu**[1,14], **Xingxing Kong**[8,14], **Makoto Fukuda**[1,7,14], **Yingfeng Deng**[2], **Eric D. Berglund**[1,3,5], **Zhuo Deng**[1,9], **Yong Gao**[1,10], **Tianya Liu**[1,11], **Jong-Woo Sohn**[1], **Lin Jia**[1], **Teppei Fujikawa**[1], **Daisuke Kohno**[1,12], **Michael M. Scott**[13], **Syann Lee**[1], **Charlotte E. Lee**[1], **Kai Sun**[2], **Yongsheng Chang**[10], **Philipp E. Scherer**[2,6,15], and **Joel K. Elmquist**[1,5,15]

[1]Division of Hypothalamic Research, The University of Texas Southwestern Medical Center at Dallas, Dallas, Texas, 75390 USA

[2]Touchstone Diabetes Center, Department of Internal Medicine, The University of Texas Southwestern Medical Center at Dallas, Dallas, Texas, 75390 USA

[3]Advanced Imaging Research Center, The University of Texas Southwestern Medical Center at Dallas, Dallas, Texas, 75390 USA

[4]Department of Neuroscience, The University of Texas Southwestern Medical Center at Dallas, Dallas, Texas, 75390 USA

[5]Department of Pharmacology, The University of Texas Southwestern Medical Center at Dallas, Dallas, Texas, 75390 USA

[6]Department of Cell Biology, The University of Texas Southwestern Medical Center at Dallas, Dallas, Texas, 75390 USA

[7]Children's Nutrition Research Center, Department of Pediatrics, Baylor College of Medicine, Houston, Texas, 77030 USA

[8]Division of Endocrinology, Beth Israel Deaconess Medical Center and Harvard Medical School, Harvard University, Boston, MA, 02115, USA

[*]Correspondence should be addressed to Kevin W. Williams Ph.D., University of Texas Southwestern Medical Center at Dallas, 5323 Harry Hines Boulevard, Dallas, Texas 75390-9077, Tel: 214-648-3771, Fax: 214-648-5612, Kevin.Williams@UTSouthwestern.edu.
[14]These authors are joint first authors.
[15]These authors are joint senior authors

Author Contributions: K.W.W., T.L., X.K. and M.F. are co-first authors. K.W.W. designed all experiments and performed all experiments except gene expression and immunoblotting, analyzed the data, and wrote the manuscript. T.L. designed and performed experiments except gene expression and immunoblotting, analyzed the data, and wrote the manuscript. X.K. analyzed gene expression in adipose depots, performed immunohistochemistry in BAT and iWAT, analyzed the data, and reviewed the manuscript. M.F. designed and performed organotypic slice experiments including immunoblotting and gene expression, analyzed data, and reviewed the manuscript. E.D.B. designed and performed hyperinsulinemic euglycemic clamp experiments, analyzed the data, and reviewed the manuscript. Y.F., J-W S., Z.D., Y.G., T.L., L.J., T.F., D.K., M.M.S., S.L., C.E.L., K.S., and Y.C. assisted performing experiments. P.E.S. and J.K.E. are co-senior authors – they supervised development of the mouse models, designed experiments, and edited the manuscript.

[9]Department of Obstetrics and Gynecology, The First Affiliated Hospital, Medical School of Xi'an Jiaotong University, Xi'an 710061, P.R. China

[10]National Laboratory of Medical Molecular Biology, Institute of Basic Medical Science, Chinese Academy of Medical Science and Peking Union Medical College, Beijing, 100005, P.R. China

[11]College of Pharmaceutical Sciences, Soochow University, Suzhou, Jiangsu 215021, China

[12]Advanced Scientific Research Leaders Development Unit, Gunma University, Maebashi, Gunma, 371-8511 Japan

[13]Department of Pharmacology, University of Virginia School of Medicine, Charlottesville, Virginia, 22908 USA

Introduction

Obesity is associated with leptin resistance (Considine et al., 1996; Frederich et al., 1995; Friedman, 2000; Morton et al., 2006; Myers et al., 2008; Myers et al., 2012), while type 2 diabetes is characterized by insulin resistance in multiple tissues (Guilherme et al., 2008; Kahn et al., 2006; Konner and Bruning, 2012; Weyer et al., 1999). Hypothalamic Pomc neurons are direct targets of both leptin and insulin contributing to their role in regulating energy expenditure, body weight, and glucose homeostasis(Belgardt and Bruning, 2010; Myers and Olson, 2012; Schwartz and Porte, 2005; Spiegelman and Flier, 2001; Williams and Elmquist, 2012; Yeo and Heisler, 2012). Recently, endoplasmic reticulum (ER) stress and the unfolded protein response (UPR) have emerged as a unifying and critical link in the development of cellular leptin and insulin resistance (Ozcan et al., 2009; Ozcan et al., 2006; Shoelson et al., 2006; Wellen and Hotamisligil, 2005; Zhang et al., 2008). In particular, obese mice and mice fed high-fat diets display ER stress in peripheral tissues as well as Pomc neurons within the hypothalamus, suggesting that metabolic disorders associated with obesity and high-fat diets induce ER stress in vivo (Schneeberger et al., 2013; Thaler et al., 2012; Xu et al., 2005). Notably, induction of ER stress or deficiency of the X-box-binding protein 1 (Xbp1) in neurons results in hyperleptinemia, obesity, hyperphagia, and reduced metabolic rate associated with severe hypothalamic leptin resistance (Ozcan et al., 2009). Additionally, ER stress suppresses leptin and insulin signaling in the periphery as well as the CNS via classical inhibitors of cytokine signaling such as the suppressor of cytokine signaling-3 (Socs3) and protein tyrosine phosphatase 1b (Ptp1b) (Howard and Flier, 2006; Myers et al., 2008; Ozcan et al., 2004; White et al., 2009; Zabolotny et al., 2008). Importantly, the neuronal cell type(s) involved in this response remains undefined. To address this issue we assessed the role of *Xbp1s* in *Pomc* neurons to regulate glucose metabolism and HFD-induced obesity. Additionally, we examined the cellular mechanisms of *Ptp1b*, *Socs3*, and *Xbp1s* in the ER stress-induced acute leptin and insulin resistance of arcuate *Pomc* neurons.

Results

Constitutive activation of *Xbp1s* in *Pomc* neurons protects against diet-induced obesity

Xbp1s improves leptin and insulin signaling along with metabolism in the periphery as well as the CNS (Deng et al., 2013; Ozcan et al., 2009; Ozcan et al., 2004; Ozcan et al., 2006). We recently developed a mouse model which expresses an inducible “dominant active” *Xbp1s* transgene via a conventional Tet-On system (Deng et al., 2013). The *Xbp1s* transgene under the control of a tetracycline-responsive element (*TRE*) supports inducible expression by the tetracycline reverse transcriptional activator (*rtTA*) in the presence of doxycycline (Dox). The *rtTA* transgene is driven by the *Rosa26* promoter with a transcriptional stop cassette flanked by 2 loxP sites upstream of *rtTA* (Belteki et al., 2005). Combined with a *Pomc* promoter–driven Cre transgene(Balthasar et al., 2004), we obtained a mouse model with *Pomc*-specific inducible expression of *Xbp1s (PIXs)*.

When fed HFD-Dox, male *PIXs* mice displayed an age-dependent lean body weight compared to wild type mice (Figure 1A), which was reflected by decreases in fat mass ($t_{(11)} = 3.965$, $p<0.05$; Figure 1B). The lean phenotype of *PIXs* was concomitant with significantly lower visceral ($t_{(11)} = 3.395$, $p<0.05$) and subcutaneous fat ($t_{(11)} = 4.090$, $p<0.05$) distribution than controls (Figures 1C and 1D). *PIXs* mice fed HFD-Dox also displayed decreased snout-anus length ($t_{(11)} = 4.928$, $p<0.05$; Supplemental Figure 1A) and decreased hepatic triglyceride ($t_{(6)} = 2.60$, $p<0.05$) and cholesterol ($t_{(6)} = 2.571$, $p<0.05$) levels (Figure 1E).

Age and weight matched *PIXs* males were hypermetabolic independent of altered food intake, as demonstrated by significant increases in energy expenditure (Figures 1F-1I and Supplemental Figure 1B). Components of total energy expenditure include energy required for physical activities and basal metabolism. In particular, *PIXs* mice exhibited increased heat production suggestive of higher metabolic rate (Figure 1I). *PIXs* mice also showed increased ambulatory movements independent of rearing activity (Figure 1J and Supplemental Figure 1C). Although we did not observe changes in ad libitum food intake, *PIXs* mice were more sensitive to acute leptin-induced hypophagia when compared to littermate controls at 4 and 6 hours after refeeding (Figure 1K).

In support of the hypermetabolic phenotype, *PIXs* mice displayed increased expression of genes associated with heat production in both brown adipose tissue - BAT (for *Ppargc1α:* $t_{(9)} = 2.957$, $p<0.05$; for *Prdm16:* $t_{(9)} = 3.691$, $p<0.05$; for *UCP1:* $t_{(9)} = 2.527$, $p<0.05$; for *Cidea:* $t_{(9)} = 2.547$, $p<0.05$; for *Dio2:* $t_{(9)} = 1.413$, $p>0.05$; for *Elovl6:* $t_{(9)} = 1.480$, $p>0.05$; Figure 2A) and inguinal white adipose tissue - iWAT (for *Ppargc1α:* $t_{(9)} = 3.289$, $p<0.05$; for *Prdm16:* $t_{(9)} = 4.158$, $p<0.05$; for *UCP1:* $t_{(9)} = 4.573$, $p<0.05$; for *Cidea:* $t_{(9)} = 4.270$, $p<0.05$; for *Dio2:* $t_{(9)} = 4.004$, $p<0.05$; for *Elovl6:* $t_{(9)} = 1.918$, $p>0.05$; Figure 2B). These data are also supported by the apparent decreased multilocular cells in BAT from *PIXs* mice (Figure 2C and 2D) and increased expression of the browning marker UCP1 in iWAT of *PIXs* mice (Figure 2E and 2F). Collectively, these results indicate that constitutive expression of *Xbp1s* in *Pomc* neurons is sufficient to improve body weight homeostasis in the context of diet-induced obesity. Moreover, *Xbp1s* in *Pomc* neurons is sufficient to

regulate metabolic rate, locomotor activity and to mediate thermogenesis (both BAT and iWAT).

Constitutive activation of *Xbp1s* in *Pomc* neurons improves insulin sensitivity and glycemia

Along with the systemic effects on whole-body energy expenditure and body weight, *Xbp1s* induction in *Pomc* neurons also leads to profound changes in glucose metabolism. *PIXs* mice fed a chow-DOX diet showed improved blood glucose levels in the fed and fasted state when compared to littermate controls (for chow dox fed *PIXs* mice: $t_{(15)} = 2.763$, $p<0.05$; for chow-DOX fasted *PIXs* mice: $t_{(15)} = 2.250$, $p<0.05$; Figure 3). Serum insulin were also decreased in *PIXs* mice during both fed and fasted conditions (for chow dox fed *PIXs* mice: $t_{(15)} = 2.217$, $p<0.05$; for chow dox fasted *PIXs* mice: $t_{(14)} = 2.515$, $p<0.05$; Figure 3).

We next performed hyperinsulinemic-euglycemic clamps to assess whether insulin sensitivity was improved in chow-fed DOX enriched *PIXs* mice compared with their littermates. Blood glucose was successfully clamped at target levels (150mg/dL; Figure 4A), and the exogenous glucose infusion rate (GIR) was higher in *PIXs* mice indicating improved insulin sensitivity (Figure 4B). This difference in GIR was due to improved insulin-mediated suppression of endogenous glucose appearance (endo R_a; Figure 4C) and not glucose disappearance (R_d; Figure 4D). Together these data suggest that constitutive expression of *Xbp1s* in Pomc neurons is sufficient to mimic a postprandial state in the liver – suppressing glucose production and ultimately lowering blood glucose levels.

Xbp1s is a cell nonautonomous feeding sensor

Upregulation of *Xbp1s* and the UDP-galactose-4-epimerase (*GalE*) in the liver maybe indicative of a fed state and contribute to metabolism (Deng et al., 2013). In support of these data, we demonstrated that both *Xbp1s* and *GalE* are upregulated in the liver after refeeding (2h) following an 18h fast (for *Xbp1s:* $t_{(8)} = 2.852$, $p<0.05$; for GalE: $t_{(8)} = 2.464$, $p<0.05$; Figure 5A). Refeeding (2h) following an 18h fast also readily elevated mRNA for both *Xbp1s* and *GalE* in the arcuate nucleus from WT mice, supporting an association of *Xbp1s-GalE* with feeding or caloric intake (for *Xbp1s:* $t_{(8)} = 3.203$, $p<0.05$; for GalE: $t_{(8)} = 3.276$, $p<0.05$; Figure 5B). Similar to our observations in refeeding after an overnight fast, Dox-containing diet induced *Xbp1s* and *GalE* mRNA as well as *Xbp1s* target genes in the Arcuate nucleus from *PIXs* mice (for *Xbp1s:* $t_{(9)} = 3.094$, $p<0.05$; for GalE: $t_{(9)} = 3.328$, $p<0.05$; for Edem1 $t(9) = 4.779$, $p<0.05$; for Erdj4 $t(9) = 2.860$, $p<0.05$; for Bip $t(9) = 3.835$, $p<0.05$; Figure 5B). The enhanced expression of *Xbp1s* and target genes was also apparent in FACs isolated *Pomc* neurons subsequent to refeeding or from FACs isolated *Pomc* from PIXs mice fed a Dox-containing diet (Figures 5C and 5D). Importantly, increased expression of *Xbp1s* mRNA levels and *Xbp1s* target genes in *Pomc* neurons from PIXs mice fed a Dox-containing diet was analogous to the elevated *Xbp1s* levels observed in *Pomc* neurons in the refed state, supporting an expression of *Xbp1s* in PIXs mice which mimicks a physiological post-prandial state. We also found that similar to recent work in C. elegans (Taylor and Dillin, 2013), constitutive expression of *Xbp1s* in murine *Pomc* neurons resulted in the transcriptional upregulation of *Xbp1s* and *Xbp1s* target genes in the liver (for *Xbp1s:* $t_{(13)} = 2.284$, $p<0.05$; for *erdj4:* $t_{(13)} = 2.477$, $p<0.05$; for *erdeml:* $t_{(13)} = 2.433$, $p<0.05$; for *chop:*

$t_{(13)} = 2.545$, $p<0.05$; for *bip:* $t_{(13)} = 1.556$, $p>0.05$; Figure 5E). Although we cannot exclude the involvement of other arms of the UPR in this cell nonautonomous regulation, the *Pomc*-dependent upregulation of Xbp1s in the liver occurred independent of detectable Cre activity within the liver. Together, these data demonstrate that Xbp1s and presumably activation of Xbp1s transcriptional targets is sufficient to signal a fed state via a cell nonautonomous regulation of the liver which may ultimately contribute to improved liver metabolic homeostasis (Deng et al., 2013).

ER stress inhibits leptin and insulin signaling in the arcuate nucleus

In an effort to identify a cellular mechanism underlying the improvements in body weight and glucose homeostasis in *PIXs* mice, we first utilized a model chronic culture system (organotypic slice preparation) recently developed in our lab (Fukuda et al., 2011; Gahwiler and Llano, 1989). Recent evidence suggests that overnutrition induces ER stress in arcuate *Pomc* neurons (Schneeberger et al., 2013). We hypothesized that ER stress may blunt leptin and insulin signaling directly in arcuate Pomc neurons. Also, constitutive expression of Xbp1s in *Pomc* neurons may improve leptin and insulin signaling in times of ER stress. Organotypic slice cultures were exposed to tunicamycin (tm), thapsigargin (tg), or dithiothreitol (dtt) in order to examine the effects of ER stress. Similar to previous observations, tm (15-30μM, 6h), tg (15μM, 6h), and dtt (1mM, 6h) suppressed the leptin-induced phosphorylation of STAT3 in the arcuate nucleus of our organotypic slice preparation (Figures 6A-6C). Notably, at 6 hours tm (30μM) and dtt (1mM) induced robust phosphorylation of the eukaryotic initiation factor 2 alpha (*eif2α*) and increased the accumulation of the ER resident molecular chaperone (*Bip/Grp78*), which are both known unfolded protein response (UPR) target genes (Supplemental Figure 2A). Additionally, tm (30μM, 6h) and dtt (1mM, 6h) potently increased mRNA for *Bip* and *CHOP/GADD153* (Supplemental Figure 2B). In addition to leptin signaling, stimulation of DMSO-treated cultures with insulin led to an increase in AKT phosphorylation (Figures 6D and 6E). Pretreatment with tm suppressed the insulin-induced phosphorylation of *AKT in* the arcuate nucleus (Figures 6D and 6E). Thus, activators of ER stress suppress the activation of multiple signaling cascades activated by leptin and insulin in the arcuate nucleus of the hypothalamus.

ER stress inhibits acute leptin and insulin signaling in arcuate *Pomc* neurons

Leptin directly activates while insulin directly inhibits arcuate *Pomc* neurons via a *PI3K* dependent mechanisms (Al-Qassab et al., 2009; Hill et al., 2008; Morton et al., 2006; Williams et al., 2010). We hypothesized that ER stress may blunt the leptin-induced activation and insulin-induced inhibition of arcuate *Pomc* neurons, which supports an ER stress-induced cellular resistance to the acute effects of leptin and insulin on metabolism.

Whole-cell recordings were performed on acute hypothalamic slices containing *Pomc*-GFP neurons within the arcuate nucleus (Parton et al., 2007; Ramadori et al., 2010). To better characterize the effects of ER stress on acute leptin and insulin signaling, we used the cre-loxP technology in order to enrich leptin responsive *Pomc* neurons in an acute hypothalamic slice preparation (Sohn et al., 2011). As expected, leptin failed to alter the membrane potential of *Pomc*-hrGFP (green) neurons that did not express *Lepr*s. In current-clamp

configuration, 75% of *Pomc*-hrGFP::*Lepr*-cre::*tdtomato* (green/red) neurons from *PLT* mice(Sohn et al., 2011) were depolarized in response to leptin (Figures 7A and 7B). Notably, none of the *Pomc*-hrGFP::*Lepr*-cre::*tdtomato* (green/red) neurons from *PLT* mice responded to insulin (supplementary table 1). A subset (40%) of *Pomc*-hrGFP neurons which did not express *Lepr*s (green cells) were hyperpolarized in response to insulin (Figures 7C and 7D), but were unresponsive to leptin (supplementary table 1). Together, these data support a model in which the acute effects of leptin and insulin are functionally segregated in distinct arcuate *Pomc* neurons. This novel model enriches the population of leptin responsive neurons in arcuate *Pomc* neurons which allows for the rapid investigation of acute ER stress-induced leptin and insulin resistance.

Pretreatment with either tm (30μM, 6h; $t_{(23)} = 8.286$, $p < 0.0001$) or tg (15μM, 6h; $t_{(21)} = 9.894$, $p < 0.0001$) blunted the ability of leptin to depolarize *Pomc*-hrGFP::*Lepr*-cre::*tdtomato* (green/red) neurons from *PLT* mice (Figures 7A and 7B). Similar to the observed blunting of acute leptin action in arcuate *Pomc* neurons pretreatment with tm (30μM, 6h; $t_{(17)} = 7.142$, $p < 0.0001$, Figures 7C and 7D) or tg (15μM, 6h; $t_{(11)} = 5.169$, $p < 0.001$, Figure 7D) blunted the ability of insulin to hyperpolarize *Pomc*-hrGFP (green) neurons from *PLT* mice. Similar results were obtained in Pomc neurons from organotypic hypothalamic slices (Supplemental Figure 3).

Cellular Mechanism for ER-stress induced acute leptin and insulin resistance in Arcuate *Pomc* neurons includes *Ptp1b, Socs3*, and *Xbp1s*

Neuronal protein tyrosine phosphatase 1b (*Ptp1b*) is required for body weight homeostasis and leptin action (Bence et al., 2006). Mice lacking *Ptp1b* selectively in *Pomc* neurons exhibited increased energy expenditure resulting in a resistance to HFD induced obesity (Banno et al., 2010). These mice were also more sensitive to the acute effect of leptin to reduce both food intake and body weight supportive of a role for *Ptp1b* in the modulation of leptin signaling involved in the acute modulation of *Pomc* cellular activity. ER stress inhibits leptin signaling via *Ptp1b* signaling in a dispersed cell culture system and in the liver (Delibegovic et al., 2009; Hosoi et al., 2008). In support of this, we found that pretreatment of hypothalamic slices with activators of ER stress resulted in increased mRNA for both *Ptp1b* and *Socs3* ($p < 0.05$; Figure 7E). Constitutive expression of *Xbp1s* in *Pomc* neurons suppressed the expression of both *Ptp1b* and *Socs3* in the Arcuate nucleus (for *Ptp1b:* $t_{(9)} = 2.371$, $p<0.05$; for *Socs3*: $t_{(9)} = 3.179$, $p<0.05$; Figure 7F). Thus, we hypothesized that *Ptp1b* and/or *Socs3* may be required in *Pomc* neurons to regulate acute ER stress induced leptin and insulin resistance. Also, *Xbp1s* alone in *Pomc* neurons may improve acute leptin and insulin signaling subsequent to ER stress.

In order to first assess the requirement of *Ptp1b* or *Socs3* in the acute ER stress-induced leptin and insulin resistance in *Pomc* neurons we generated *Pomc* reporter mice by mating *Pomc*-cre mice with the tdtomato reporter mouse (Jackson Laboratory, #007908). Similar to previous reports (Al-Qassab et al., 2009; Hill et al., 2008; Williams et al., 2010), *Pomc* neurons from *Pomc*-cre::tdtomato mice were activated in response to leptin and inhibited in response to insulin (Figures 7B and 7D). *Pomc*-cre::tdtomato reporter mice were subsequently mated to either Ptp1b-lox (*Pomc*-cre::tdtomato::Ptp1b-lox) or *Socs3*-lox

(*Pomc*-cre::tdtomato::*Socs3*-lox) mice. Tunicamycin failed to blunt the leptin-induced activation of *Pomc* neurons selectively deficient for either Ptp1b or *Socs3* (for *Pomc*-cre::tdtomato::Ptp1b-lox $t_{(18)} = 1.918$, $p > 0.05$; for *Pomc*-cre::tdtomato::*Socs3*-lox $t_{(18)} = 1.167$, $p > 0.05$; Figure 7B). Similarly, tunicamycin failed to blunt the insulin-induced inhibition of *Pomc* neurons selectively deficient for either *Ptp1b* (for *Pomc*-cre::tdtomato::*Ptp1b*-lox $t_{(14)} = 0.9115$, $p > 0.05$; Figure 7D). Notably, *Pomc* neurons deficient for *Socs3* were significantly more responsive to insulin compared to *Pomc* neurons deficient for *Ptp1b* alone or control mice (for insulin in *Pomc*-cre::tdtomato::*Socs3*-lox cells compared to *Pomc*-cre::tdtomato::*Ptp1b*-lox mice $t_{(12)} = 4.457$, $p < 0.05$; for insulin in *Pomc*-cre::tdtomato::*Socs3*-lox cells compared to control PLT mice $t_{(14)} = 3.849$, $p < 0.05$ Figure 7D). Although ER stress stimulates both *Ptp1b* and *Socs3* (Figure 7E), these data suggest that *Soc3* may have a more potent ER stress induced activity related to the suppression of acute leptin and insulin signaling in arcuate *Pomc* neurons.

In order to assess the role of *Xbp1s* in the acute ER stress-induced leptin and insulin resistance, *Pomc* reporter *PIXs* mice were generated by mating PIXs mice with tdtomato reporter mouse (Jackson Laboratory, #007908). Tunicamycin failed to blunt the leptin-induced activation of *Pomc* neurons from *PIXs* mice fed a doxycycline enriched diet ($t_{(19)} = 1.320$, $p > 0.05$; Figure 7B). Similarly, tunicamycin failed to blunt the insulin-induced inhibition of *Pomc* neurons from *PIXs* mice fed a doxycycline enriched diet ($t_{(17)} = 0.3917$, $p > 0.05$; Figure 7D).

Discussion

Constitutive expression of *Xbp1s* in *Pomc* neurons (*PIXs* mice) increases energy expenditure, desensitizes mice to diet-induced obesity independent of changes in ad-libitum food intake, and directly (i.e. independently of changes in body weight) improves glucose homeostasis with decreases in circulating insulin and blood glucose. In addition to these physiological aberrations, *PIXs* mice were sensitized the acute effects of leptin pharmacologically to suppress food intake. On a cellular level, *PIXs* mice exhibited decreased *Ptp1b* and *Socs3* expression concomitant with improved leptin and insulin signaling in *Pomc* neurons subsequent to ER stress. Increased *XBP1s* expression only in *Pomc* neurons was sufficient to upregulate of the *XBP1s* axis in the liver. Together, these data support a model in which a “fed” signal in *Pomc* neurons abrogates high-fat diet induced obesity while at the same time induces a “fed” transcriptional program in the liver improving glucose homeostasis.

ER stress pathways in Pomc neurons regulates hepatic glucose production. It is of particular interest that *Xbp1s* expression in *Pomc* neurons has profound effects on body weight and glucose homeostasis. Cellular stress and inflammatory pathways including ER stress and the UPR have been linked to leptin and insulin resistance as well as obesity and diabetes (Kaneto et al., 2005; Tsiotra and Tsigos, 2006; Wellen and Hotamisligil, 2005). Notably, *Xbp-1*$^{+/-}$ heterozygous mice are more sensitive to diabetes caused by obesity and high-fat diet (Ozcan et al., 2004). Similar results were obtained in mice deficient for *Xbp1s* selectively in neurons (Ozcan et al., 2009). The decreased body weight observed in mice which constitutively express *Xbp1s* in *Pomc* neurons was dependent upon a hypermetabolic

phenotype (increased energy expenditure and heat production) independent of altered food intake. Notably, these responses are phenotypic signatures of improved leptin action within *Pomc* neurons (Balthasar et al., 2004; Berglund et al., 2012; Williams et al., 2011). The hypermetabolic phenotype was also supported by increased markers for thermogenesis in BAT as well as iWAT (Cypess et al., 2009; van Marken Lichtenbelt et al., 2009; Virtanen et al., 2009; Wu et al., 2012). The increased thermogenesis of iWAT suggests that *Xbp1s* expression in *Pomc* neurons promotes browning/beiging of white adipose tissues contributing to improvements in body weight. Similar to *Xbp1s* activity in the liver (Deng et al., 2013), we found that constitutive expression of *Xbp1s* in *Pomc* neurons alone was also sufficient to improve blood glucose and insulin levels, supportive of improved insulin signaling and reminiscent of a fed state even in the absence of caloric intake.

A neuronal cell non-autonomous regulation of Xbp1 transcription in the intestinal cell of C. elegans has recently been described (Taylor and Dillin Cell 2013). Notably, the improved glucoregulation in the current study may be due to elevated Xbp1s levels in the liver via a similar cell nonautonomous mechanism. Hypothalamic neuronal regulation of peripheral tissues such as liver and pancreas is likely due to hypothalamic regulation of the activity of key autonomic control neurons in the brainstem and spinal cord. Although, this occurs via multisynaptic connections that may involve melanocortin 4 receptor expressing neurons in key autonomic circuits (Rossi et al., 2011; Sohn et al., 2013), it's currently unclear how Pomc neurons propagate the Xbp1s transcriptional signal to the liver.

Another salient finding is the relationship between *Xbp1s* and both *Ptp1b* and *Socs3* in the ER stress induced acute leptin and insulin resistance of Arcuate *Pomc* neurons. Recently, ER stress has been shown to induce leptin resistance within the hypothalamus as well as peripheral insulin resistance in the liver and muscle (Ozcan et al., 2009; Ozcan et al., 2006; Thaler and Schwartz, 2010; Thaler et al., 2012). In the current study, our findings point to a fundamental role of ER-stress in regulating leptin and insulin signaling in hypothalamic *Pomc* neurons. Classical suppressors of cytokine signaling have been likely candidates in ER stress induced leptin and insulin resistance (Howard and Flier, 2006; Myers et al., 2008; White et al., 2008; Zabolotny et al., 2008) . In particular, both *Socs3* and *Ptp1b* are increased within the hypothalamus in a state of excess nutrition or obesity (Bjorbaek et al., 1998; Enriori et al., 2007; Munzberg et al., 2004; White et al., 2008; Zabolotny et al., 2008). Brain specific *Socs3* knockout mice or haploinsufficient mice were significantly protected against the development of DIO associated with leptin resistance (Howard et al., 2004; Mori et al., 2004). *Ptp1b* knockout mice were similarly resistant to DIO (Bence et al., 2006; Cook and Unger, 2002; Zabolotny et al., 2002). Notably, both *Ptp1b* and *Socs3* can be induced by non-cytokine stimuli, including ER stress (Hosoi et al., 2008; Ozcan et al., 2009; Yoshimura et al., 2007; Zhang et al., 2008). *Ptp1b* also mediates ER stress-induced hypothalamic leptin resistance independent of *Socs3* activity (Hosoi et al., 2008). Recently, liver specific deficiency of *Ptp1b* attenuated the induction of ER stress in response to high-fat diet (Delibegovic et al., 2009). These data are supported in the current study with the demonstration that ER stress stimulates *Ptp1b* and *Socs3* in the arcuate nucleus of the hypothalamus. *Pomc* neurons selectively deficient for either *Ptp1b* or *Socs3* demonstrated improved acute leptin and insulin signaling subsequent to ER stress activation. Constitutive

expression of *Xbp1s* in *Pomc* neurons lowered mRNA levels of *Ptp1b* and *Socs3* at the same time blunting the ability of strong inducers of ER stress to induce cellular leptin and insulin resistance in *Pomc* neurons. It should be noted that several groups have reported that ER stress stimulates the production and phosphatase activity of PTP1B and Socs3 in multiple tissues (Agouni et al., 2011; Bettaieb et al., 2011; Hosoi et al., 2008; Panzhinskiy et al., 2013). However, it has been unclear how ER stress induced PTP1B or SOCS3 activity may affect acute hypothalamic leptin and insulin signaling. In particular, PTP1B has been suggested to operate as a component of the UPRosome, selectively controlling IRE1 activation and signaling (Gu et al., 2004). These data suggest the PTP1b dependent ER stress induced acute leptin and insulin resistance in the current study may be explained by a lack of IRE1-XBP1 activation. In contrast, ER stress-induced sulfhydration of PTP1B inhibits it's native activity and thereby promotes PERK activity during the response to ER stress(Krishnan et al., 2011). Thus although it is apparent that PTP1B activity is intertwined with ER stress and the UPR, the current study extends previous observations and supports a requirement of PTP1B and SOCS3 in ER stress-induced acute leptin and insulin resistance of POMC neurons.

Overall, these observations underscore a physiologically important role for ER stress and the UPR to alter the ability of arcuate *Pomc* neurons to properly respond to humoral signals. ultimately abrogating diet-induced obesity and diabetes. Notably, the improvements in leptin and insulin signaling observed in the current study during times of ER stress link *Xbp1s* with both *Ptp1b* and *Socs3* in *Pomc* neurons. These data also demonstrate that *Pomc* neurons induce changes in the metabolic flux in the liver in a cell nonautonomous mechanism which contributes to improved glucose homeostasis independent of altered body weight. In addition, these data clarify the roles of these molecules in the regulation of metabolism and may highlight useful targets for regulating obesity and related metabolic disorders.

Experimental Procedures

Animals

Male (4- 16-week-old) pathogen-free POMC-hrGFP mice(Parton et al., 2007; Ramadori et al., 2010) were used for all experiments. To identify POMC neurons with or without leptin receptors, we generated PLT mice as previously described(Sohn et al., 2011). Briefly, LepR reporter mice were made by mating LepR-cre mice(Scott et al., 2009) with the tdtomato reporter mouse (Jackson Laboratory, #007908). LepR-cre::tdtomato reporter mice were subsequently mated with POMC-hrGFP mice to produce POMC::LepR-cre::tdtomato (PLT) mice. To identify Pomc neurons with or without Ptp1b or Socs3, we generated Pomc-cre::tdtomato::Ptp1b lox or Pomc-cre::tdtomato::Socs3 lox mice, respectively. Briefly, Pomc-cre reporter mice were made by mating Pomc-cre mice with the tdtomato reporter mouse. Pomc-cre::tdtomato mice were subsequently mated with either Ptp1b lox or Socs3 lox mice. Subsequent matings generated mice that were deficient for either Ptp1b or Socs3 in Pomc neurons.

All mice were housed under standard laboratory conditions (12 hr on/off; lights on at 7:00 a.m.) and temperature-controlled environment with food and water available ad libitum. All experiments were performed in accordance with the guidelines established by the National

Institute of Health Guide for the Care and Use of Laboratory Animals, and approved by the University of Texas Institutional Animal Care and Use Committee.

Western Blot Analysis

The arcuate nucleus was microdissected with a scalpel under a microscope age matched male mice. Whole cell proteins were extracted by homogenizing the hypothalamic blocks in IP Lysis buffer [25mM Tris-HCl pH 7.4, 150mM NaCl, 1mM EDTA, 1% NP-40 and 5% glycerol (87787 Pierce)], with protease and phosphatase inhibitors cocktails (1:100, 78440, Pierce). Equal amounts of the samples (10 μg) were separated by SDS-PAGE and transferred to a nitrocellulose membrane by electroblotting. Antibodies used here are the following: A phospho-STAT3 antibody (1:1,000, Cell Signaling Technology, 9131), a phospho-ERK antibody (1:1,000, Cell Signaling Technology, 4370), an antibody against STAT3 (1:1,000, Cell Signaling Technology, 9139), pAKT (1:1,000, Cell Signaling, # 4060), AKT (1:1,000, Cell Signaling, # 4691), an antibody against SOCS3 (1:600, Abcam, ab16030), a PTP1B antibody (1:333, Abcam, ab52650), Bip (1:1,000, Chop Cell Signaling Technology, 3177), eif2α (1:1,000, Cell Signaling, # 3398), XBP1 (1:200, Santa Cruz Biotechnology Inc, SC-7160), and anti β-actin antibodies (1:10,000, beta Actin antibody, mAbcam 8226). After incubation in primary antibodies for 72 h, the membranes were incubated for 1 h in HRP-conjugated secondary antibodies (1:7,000, Southern Biotech, 1010-05 and 4050-05), followed by chemiluminescent detection using West Pico Chemiluminescent Substrate (Thermo Fisher Scientific Inc.). To measure the fluorescent intensity, the Odyssey IR imaging system (LI-COR Biosciences) was used. After incubation for primary antibodies, the membrane was incubated in the secondary antibody conjugated to a fluorescent entity: IRDye 800-conjugated goat antirabbit IgG and/or Alexa Fluor 680-conjugated goat antimouse IgG (dilution 1:10,000) with gentle agitation for 1 h at room temperature. At the end of the incubation period, membranes were washed twice with phosphate -buffered saline (PBS) with 0.05% Tween (PBS-T). The membrane was visualized and analyzed on the Odyssey IR imaging system (LI-COR Biosciences). Phospho-proteins were normalized to the levels of the corresponding total protein.

Electrophysiology

Whole-cell patch-clamp recordings from POMC-hrGFP neurons maintained in hypothalamic slice preparations and data analysis were performed as previously described(Hill et al., 2008). Briefly, 4- to 16-week-old male mice were anesthetized and transcardially perfused with a modified ice-cold artificial CSF (ACSF) (described below), in which an equiosmolar amount of sucrose was substituted for NaCl. The mice were then decapitated, and the entire brain was removed, and immediately submerged in ice-cold, carbogen-saturated (95% O2 and 5% CO2) ACSF (126 mM NaCl, 2.8 mM KCl, 1.2 mM MgCl2, 2.5 mM CaCl2, 1.25 mM NaH2PO4, 26 mM NaHCO3, and 5 mM glucose). Coronal sections (250 μm) were cut with a Leica VT1000S Vibratome and then incubated in oxygenated ACSF at room temperature for at least 1 hr before recording. Slices were transferred to the recording chamber and allowed to equilibrate for 10–20 min before recording. The slices were bathed in oxygenated ACSF (32°C–34°C) at a flow rate of ∼2 ml/min.

The pipette solution for whole-cell recording was modified to include an intracellular dye (Alexa Fluor 594 or Alexa Fluor 350) for whole-cell recording: 120 mM K-gluconate, 10 mM KCl, 10 mM HEPES, 5 mM EGTA, 1 mM CaCl2, 1 mM MgCl2, and 2 mM MgATP, 0.03 mM Alexa Fluor 594 or Alexa Fluor 350 hydrazide dye (pH 7.3). Epifluorescence was briefly used to target fluorescent cells, at which time the light source was switched to infrared differential interference contrast imaging to obtain the whole-cell recording (Zeiss Axioskop FS2 Plus equipped with a fixed stage and a QuantEM:512SC electron-multiplying charge-coupled device camera). Electrophysiological signals were recorded using an Axopatch 700B amplifier (Molecular Devices), low-pass filtered at 2–5 kHz, and analyzed offline on a PC with pCLAMP programs (Molecular Devices). Recording electrodes had resistances of 2.5–5 MΩ when filled with the K-gluconate internal solution. Input resistance was assessed by measuring voltage deflection at the end of the response to a hyperpolarizing rectangular current pulse steps (500 ms of −10 to −50 pA).

Leptin (100 nM; provided by A.F. Parlow, through the National Hormone and Peptide Program) or insulin (50 nM, Humulin-R 100 U/ml; Lilly), were added to the ACSF for specific experiments. Solutions containing leptin or insulin were typically perfused for 2–4 min. A drug effect was required to be associated temporally with peptide application, and the response had to be stable within a few minutes. A neuron was considered depolarized or hyperpolarized if a change in membrane potential was at least 2 mV in amplitude.

Energy expenditure and locomotor activity

Weight- and body composition–matched 8-week-old WT and *PIXs* mice were used for metabolic assessment. Three separate cohorts of animals were used to produce the metabolic data, with measurements sorted into 12-hour-light/dark periods. To exclude the possibility that changes in body weight or composition would contribute to energy expenditure measurements, metabolic assessment was done using weight- and body composition–matched mice(Butler and Kozak, 2010; Tschop et al., 2012). Data, where applicable, were also normalized to lean body mass, by raising metabolic data to the power of ×0.75 (or by expressing data on a per animal basis)(Butler and Kozak, 2010; Tschop et al., 2012).

Mice were first acclimatized to the metabolic cages and housed individually for 4 days before measurements were taken. Mice were analyzed in the metabolic chambers for 4 days and were provided with food ad libitum. Energy expenditure was measured by indirect calorimetry, while locomotor activity was assessed using an infrared light beam detection system (Labmaster, TSE Systems GmbH). Data was collected using a TSE Labmaster monitoring system (TSE Systems GmbH). Locomotor activity and energy expenditure were determined for both the 12-hour-light and 12-hour-dark cycle as well as for the whole 24-hour period. Data were averaged over the 4-day period of measurement.

Body weight/composition, and fat distribution

Animals were weaned and maintained on a high-fat diet enriched with doxycycline (600mg/kg) at 4 to 5 weeks of age. Body weight was measured weekly up to 25 weeks. Body fat composition of 25-week-old ad libitum fed mice was assessed using nuclear magnetic resonance spectroscopy using an NMR spectrometer (EchoMRI). For fat

distribution, mice were anesthetized with 1% isoflurane inhalation and then the trunk (from base of the skull as the spinal canal begins to widen and the distal end of the tibia) of each mouse was scanned at an isotropic voxel size of 93 μm (80 kV, 450 μA, and 100 ms integration time) using the eXplore Locus micro-CT scanner (GE Health Care). Three-dimensional images were reconstructed from two-dimensional grayscale image slices and visualized using Microview Software (GE Medical System). Density values for soft tissue and bone were calibrated from a phantom (GE Health Care) containing air bubble, water, and hydroxyl apatite rod. The separation of fat regions was obtained from the appropriate grayscale value (upper threshold, −165; lower threshold, −360). The abdominal muscular wall was used as the differentiation line to separate visceral adipose tissue from subcutaneous adipose tissue. The contour lines were drawn around the viscera and three-dimensional ROI was generated. The visceral fat was determined from the histogram of these segmented viscera using the same thresholds. Subcutaneous fat was obtained by subtracting visceral fat from the total body fat.

Data Analysis

Statistical analysis was carried out using GraphPad 5 (GraphPad) software. All data were evaluated using a 2-tailed Student's *t* test with a *P* value of less than 0.05 being considered significant. In all instances, data are presented as mean ± SEM. Body weight curves were compared using a linear regression analysis. . Degrees of freedom (DF) for *t* statistics are marked as $t_{(DF)}$.

Supplementary Material

Refer to Web version on PubMed Central for supplementary material.

Acknowledgments

We thank Dr. Jeffrey Friedman (Rockefeller University) for kindly providing us with the *Lepr*-cre mice. We also thank Dr. Bradford Lowell (Beth Israel Deaconess Medical Center) for kindly providing us with the *Pomc*-hrGFP mice. This work was supported by grants to K.W.W. (K01DK087780), T.L. (American Diabetes Association 7-11-MN-16), M.F. (American Heart Association – 9SDG2080223), J.-W.S. (American Heart Association 12POST8860007), Y.D. (American Diabetes Association 7-08-MN-53), E.D.B. (NIH F32 DK092083 and K01 DK098317), X.K. (American Heart Association 13POST16710016), T.F. (Juvenile Diabetes Research Foundation – 3-2011-405), and J.K.E. (R01DK53301, R01DK088423, and RL1DK081185). This work was also supported by PL1 DK081182 and UL1RR024923, as well as P01DK088761 (P.E.S. and J.K.E.) and R01DK55758 (P.E.S.).

References

Agouni A, Mody N, Owen C, Czopek A, Zimmer D, Bentires-Alj M, Bence KK, Delibegovic M. Liver-specific deletion of protein tyrosine phosphatase (PTP) 1B improves obesity- and pharmacologically induced endoplasmic reticulum stress. Biochem J. 2011; 438:369–378. [PubMed: 21605081]

Al-Qassab H, Smith MA, Irvine EE, Guillermet-Guibert J, Claret M, Choudhury AI, Selman C, Piipari K, Clements M, Lingard S, et al. Dominant role of the p110beta isoform of PI3K over p110alpha in energy homeostasis regulation by POMC and AgRP neurons. Cell Metab. 2009; 10:343–354. [PubMed: 19883613]

Balthasar N, Coppari R, McMinn J, Liu SM, Lee CE, Tang V, Kenny CD, McGovern RA, Chua SC Jr, Elmquist JK, et al. Leptin receptor signaling in POMC neurons is required for normal body weight homeostasis. Neuron. 2004; 42:983–991. [PubMed: 15207242]

Banno R, Zimmer D, De Jonghe BC, Atienza M, Rak K, Yang W, Bence KK. PTP1B and SHP2 in POMC neurons reciprocally regulate energy balance in mice. The Journal of clinical investigation. 2010; 120:720–734. [PubMed: 20160350]

Belgardt BF, Bruning JC. CNS leptin and insulin action in the control of energy homeostasis. Annals of the New York Academy of Sciences. 2010; 1212:97–113. [PubMed: 21070248]

Belteki G, Haigh J, Kabacs N, Haigh K, Sison K, Costantini F, Whitsett J, Quaggin SE, Nagy A. Conditional and inducible transgene expression in mice through the combinatorial use of Cre-mediated recombination and tetracycline induction. Nucleic Acids Res. 2005; 33:e51. [PubMed: 15784609]

Bence KK, Delibegovic M, Xue B, Gorgun CZ, Hotamisligil GS, Neel BG, Kahn BB. Neuronal PTP1B regulates body weight, adiposity and leptin action. Nat Med. 2006; 12:917–924. [PubMed: 16845389]

Berglund ED, Vianna CR, Donato J Jr, Kim MH, Chuang JC, Lee CE, Lauzon DA, Lin P, Brule LJ, Scott MM, et al. Direct leptin action on POMC neurons regulates glucose homeostasis and hepatic insulin sensitivity in mice. The Journal of clinical investigation. 2012; 122:1000–1009. [PubMed: 22326958]

Bettaieb A, Liu S, Xi Y, Nagata N, Matsuo K, Matsuo I, Chahed S, Bakke J, Keilhack H, Tiganis T, et al. Differential regulation of endoplasmic reticulum stress by protein tyrosine phosphatase 1B and T cell protein tyrosine phosphatase. J Biol Chem. 2011; 286:9225–9235. [PubMed: 21216966]

Bjorbaek C, Elmquist JK, Frantz JD, Shoelson SE, Flier JS. Identification of SOCS-3 as a potential mediator of central leptin resistance. Mol Cell. 1998; 1:619–625. [PubMed: 9660946]

Bookout AL, Mangelsdorf DJ. Quantitative real-time PCR protocol for analysis of nuclear receptor signaling pathways. Nucl Recept Signal. 2003; 1:e012. [PubMed: 16604184]

Butler AA, Kozak LP. A recurring problem with the analysis of energy expenditure in genetic models expressing lean and obese phenotypes. Diabetes. 2010; 59:323–329. [PubMed: 20103710]

Considine RV, Sinha MK, Heiman ML, Kriauciunas A, Stephens TW, Nyce MR, Ohannesian JP, Marco CC, McKee LJ, Bauer TL, et al. Serum immunoreactive-leptin concentrations in normal-weight and obese humans. The New England journal of medicine. 1996; 334:292–295. [PubMed: 8532024]

Cook WS, Unger RH. Protein tyrosine phosphatase 1B: a potential leptin resistance factor of obesity. Dev Cell. 2002; 2:385–387. [PubMed: 11970889]

Cravo RM, Margatho LO, Osborne-Lawrence S, Donato J Jr, Atkin S, Bookout AL, Rovinsky S, Frazao R, Lee CE, Gautron L, et al. Characterization of Kiss1 neurons using transgenic mouse models. Neuroscience. 2011; 173:37–56. [PubMed: 21093546]

Cypess AM, Lehman S, Williams G, Tal I, Rodman D, Goldfine AB, Kuo FC, Palmer EL, Tseng YH, Doria A, et al. Identification and importance of brown adipose tissue in adult humans. The New England journal of medicine. 2009; 360:1509–1517. [PubMed: 19357406]

Delibegovic M, Zimmer D, Kauffman C, Rak K, Hong EG, Cho YR, Kim JK, Kahn BB, Neel BG, Bence KK. Liver-specific deletion of protein-tyrosine phosphatase 1B (PTP1B) improves metabolic syndrome and attenuates diet-induced endoplasmic reticulum stress. Diabetes. 2009; 58:590–599. [PubMed: 19074988]

Deng Y, Wang ZV, Tao C, Gao N, Holland WL, Ferdous A, Repa JJ, Liang G, Ye J, Lehrman MA, et al. The Xbp1s/GalE axis links ER stress to postprandial hepatic metabolism. The Journal of clinical investigation. 2013; 123:455–468. [PubMed: 23257357]

Enriori PJ, Evans AE, Sinnayah P, Jobst EE, Tonelli-Lemos L, Billes SK, Glavas MM, Grayson BE, Perello M, Nillni EA, et al. Diet-induced obesity causes severe but reversible leptin resistance in arcuate melanocortin neurons. Cell Metab. 2007; 5:181–194. [PubMed: 17339026]

Frederich RC, Hamann A, Anderson S, Lollmann B, Lowell BB, Flier JS. Leptin levels reflect body lipid content in mice: evidence for diet-induced resistance to leptin action. Nat Med. 1995; 1:1311–1314. [PubMed: 7489415]

Friedman JM. Obesity in the new millennium. Nature. 2000; 404:632–634. [PubMed: 10766249]

Fukuda M, Jones JE, Olson D, Hill J, Lee CE, Gautron L, Choi M, Zigman JM, Lowell BB, Elmquist JK. Monitoring FoxO1 localization in chemically identified neurons. J Neurosci. 2008; 28:13640–13648. [PubMed: 19074037]

Fukuda M, Williams KW, Gautron L, Elmquist JK. Induction of leptin resistance by activation of cAMP-Epac signaling. Cell Metab. 2011; 13:331–339. [PubMed: 21356522]

Gahwiler BH, Llano I. Sodium and potassium conductances in somatic membranes of rat Purkinje cells from organotypic cerebellar cultures. J Physiol. 1989; 417:105–122. [PubMed: 2559965]

Gu F, Nguyen DT, Stuible M, Dube N, Tremblay ML, Chevet E. Protein-tyrosine phosphatase 1B potentiates IRE1 signaling during endoplasmic reticulum stress. J Biol Chem. 2004; 279:49689–49693. [PubMed: 15465829]

Guilherme A, Virbasius JV, Puri V, Czech MP. Adipocyte dysfunctions linking obesity to insulin resistance and type 2 diabetes. Nat Rev Mol Cell Biol. 2008; 9:367–377. [PubMed: 18401346]

Hill JW, Elias CF, Fukuda M, Williams KW, Berglund ED, Holland WL, Cho YR, Chuang JC, Xu Y, Choi M, et al. Direct insulin and leptin action on pro-opiomelanocortin neurons is required for normal glucose homeostasis and fertility. Cell Metab. 2010; 11:286–297. [PubMed: 20374961]

Hill JW, Williams KW, Ye C, Luo J, Balthasar N, Coppari R, Cowley MA, Cantley LC, Lowell BB, Elmquist JK. Acute effects of leptin require PI3K signaling in hypothalamic proopiomelanocortin neurons in mice. The Journal of clinical investigation. 2008; 118:1796–1805. [PubMed: 18382766]

Hosoi T, Sasaki M, Miyahara T, Hashimoto C, Matsuo S, Yoshii M, Ozawa K. Endoplasmic reticulum stress induces leptin resistance. Mol Pharmacol. 2008; 74:1610–1619. [PubMed: 18755873]

Howard JK, Cave BJ, Oksanen LJ, Tzameli I, Bjorbaek C, Flier JS. Enhanced leptin sensitivity and attenuation of diet-induced obesity in mice with haploinsufficiency of Socs3. Nat Med. 2004; 10:734–738. [PubMed: 15220914]

Howard JK, Flier JS. Attenuation of leptin and insulin signaling by SOCS proteins. Trends Endocrinol Metab. 2006; 17:365–371. [PubMed: 17010638]

Kahn SE, Hull RL, Utzschneider KM. Mechanisms linking obesity to insulin resistance and type 2 diabetes. Nature. 2006; 444:840–846. [PubMed: 17167471]

Kaneto H, Nakatani Y, Kawamori D, Miyatsuka T, Matsuoka TA, Matsuhisa M, Yamasaki Y. Role of oxidative stress, endoplasmic reticulum stress, and c-Jun N-terminal kinase in pancreatic beta-cell dysfunction and insulin resistance. The international journal of biochemistry & cell biology. 2005; 37:1595–1608. [PubMed: 15878838]

Konner AC, Bruning JC. Selective insulin and leptin resistance in metabolic disorders. Cell Metab. 2012; 16:144–152. [PubMed: 22883229]

Krishnan N, Fu C, Pappin DJ, Tonks NK. H2S-Induced sulfhydration of the phosphatase PTP1B and its role in the endoplasmic reticulum stress response. Sci Signal. 2011; 4:ra86. [PubMed: 22169477]

Mao X, Fujiwara Y, Chapdelaine A, Yang H, Orkin SH. Activation of EGFP expression by Cre-mediated excision in a new ROSA26 reporter mouse strain. Blood. 2001; 97:324–326. [PubMed: 11133778]

Mori H, Hanada R, Hanada T, Aki D, Mashima R, Nishinakamura H, Torisu T, Chien KR, Yasukawa H, Yoshimura A. Socs3 deficiency in the brain elevates leptin sensitivity and confers resistance to diet-induced obesity. Nat Med. 2004; 10:739–743. [PubMed: 15208705]

Morton GJ, Cummings DE, Baskin DG, Barsh GS, Schwartz MW. Central nervous system control of food intake and body weight. Nature. 2006; 443:289–295. [PubMed: 16988703]

Munzberg H, Flier JS, Bjorbaek C. Region-specific leptin resistance within the hypothalamus of diet-induced obese mice. Endocrinology. 2004; 145:4880–4889. [PubMed: 15271881]

Myers MG, Cowley MA, Munzberg H. Mechanisms of leptin action and leptin resistance. Annu Rev Physiol. 2008; 70:537–556. [PubMed: 17937601]

Myers MG Jr, Heymsfield SB, Haft C, Kahn BB, Laughlin M, Leibel RL, Tschop MH, Yanovski JA. Challenges and opportunities of defining clinical leptin resistance. Cell Metab. 2012; 15:150–156. [PubMed: 22326217]

Myers MG Jr, Olson DP. Central nervous system control of metabolism. Nature. 2012; 491:357–363. [PubMed: 23151578]

Ozcan L, Ergin AS, Lu A, Chung J, Sarkar S, Nie D, Myers MG Jr, Ozcan U. Endoplasmic reticulum stress plays a central role in development of leptin resistance. Cell Metab. 2009; 9:35–51. [PubMed: 19117545]

Ozcan U, Cao Q, Yilmaz E, Lee AH, Iwakoshi NN, Ozdelen E, Tuncman G, Gorgun C, Glimcher LH, Hotamisligil GS. Endoplasmic reticulum stress links obesity, insulin action, and type 2 diabetes. Science (New York, NY). 2004; 306:457–461.

Ozcan U, Yilmaz E, Ozcan L, Furuhashi M, Vaillancourt E, Smith RO, Gorgun CZ, Hotamisligil GS. Chemical chaperones reduce ER stress and restore glucose homeostasis in a mouse model of type 2 diabetes. Science (New York, NY). 2006; 313:1137–1140.

Panzhinskiy E, Hua Y, Culver B, Ren J, Nair S. Endoplasmic reticulum stress upregulates protein tyrosine phosphatase 1B and impairs glucose uptake in cultured myotubes. Diabetologia. 2013; 56:598–607. [PubMed: 23178931]

Parton LE, Ye CP, Coppari R, Enriori PJ, Choi B, Zhang CY, Xu C, Vianna CR, Balthasar N, Lee CE, et al. Glucose sensing by POMC neurons regulates glucose homeostasis and is impaired in obesity. Nature. 2007; 449:228–232. [PubMed: 17728716]

Ramadori G, Fujikawa T, Fukuda M, Anderson J, Morgan DA, Mostoslavsky R, Stuart RC, Perello M, Vianna CR, Nillni EA, et al. SIRT1 deacetylase in POMC neurons is required for homeostatic defenses against diet-induced obesity. Cell Metab. 2010; 12:78–87. [PubMed: 20620997]

Rossi J, Balthasar N, Olson D, Scott M, Berglund E, Lee CE, Choi MJ, Lauzon D, Lowell BB, Elmquist JK. Melanocortin-4 receptors expressed by cholinergic neurons regulate energy balance and glucose homeostasis. Cell Metabolism. 2011; 13:195–204. [PubMed: 21284986]

Schneeberger M, Dietrich MO, Sebastian D, Imbernon M, Castano C, Garcia A, Esteban Y, Gonzalez-Franquesa A, Rodriguez IC, Bortolozzi A, et al. Mitofusin 2 in POMC neurons connects ER stress with leptin resistance and energy imbalance. Cell. 2013; 155:172–187. [PubMed: 24074867]

Schwartz MW, Porte D Jr. Diabetes, obesity, and the brain. Science (New York, NY). 2005; 307:375–379.

Scott MM, Lachey JL, Sternson SM, Lee CE, Elias CF, Friedman JM, Elmquist JK. Leptin targets in the mouse brain. J Comp Neurol. 2009; 514:518–532. [PubMed: 19350671]

Shoelson SE, Lee J, Goldfine AB. Inflammation and insulin resistance. The Journal of clinical investigation. 2006; 116:1793–1801. [PubMed: 16823477]

Sohn JW, Harris LE, Berglund ED, Liu T, Vong L, Lowell BB, Balthasar N, Williams KW, Elmquist JK. Melanocortin 4 receptors reciprocally regulate sympathetic and parasympathetic preganglionic neurons. Cell. 2013; 152:612–619. [PubMed: 23374353]

Sohn JW, Xu Y, Jones JE, Wickman K, Williams KW, Elmquist JK. Serotonin 2C receptor activates a distinct population of arcuate pro-opiomelanocortin neurons via TRPC channels. Neuron. 2011; 71:488–497. [PubMed: 21835345]

Spiegelman BM, Flier JS. Obesity and the regulation of energy balance. Cell. 2001; 104:531–543. [PubMed: 11239410]

Taylor RC, Dillin A. XBP-1 is a cell-nonautonomous regulator of stress resistance and longevity. Cell. 2013; 153:1435–1447. [PubMed: 23791175]

Thaler JP, Schwartz MW. Minireview: Inflammation and obesity pathogenesis: the hypothalamus heats up. Endocrinology. 2010; 151:4109–4115. [PubMed: 20573720]

Thaler JP, Yi CX, Schur EA, Guyenet SJ, Hwang BH, Dietrich MO, Zhao X, Sarruf DA, Izgur V, Maravilla KR, et al. Obesity is associated with hypothalamic injury in rodents and humans. The Journal of clinical investigation. 2012; 122:153–162. [PubMed: 22201683]

Tschop MH, Speakman JR, Arch JR, Auwerx J, Bruning JC, Chan L, Eckel RH, Farese RV Jr, Galgani JE, Hambly C, et al. A guide to analysis of mouse energy metabolism. Nat Methods. 2012; 9:57–63. [PubMed: 22205519]

Tsiotra PC, Tsigos C. Stress, the endoplasmic reticulum, and insulin resistance. Annals of the New York Academy of Sciences. 2006; 1083:63–76. [PubMed: 17148734]

van Marken Lichtenbelt WD, Vanhommerig JW, Smulders NM, Drossaerts JM, Kemerink GJ, Bouvy ND, Schrauwen P, Teule GJ. Cold-activated brown adipose tissue in healthy men. The New England journal of medicine. 2009; 360:1500–1508. [PubMed: 19357405]

Virtanen KA, Lidell ME, Orava J, Heglind M, Westergren R, Niemi T, Taittonen M, Laine J, Savisto NJ, Enerback S, et al. Functional brown adipose tissue in healthy adults. The New England journal of medicine. 2009; 360:1518–1525. [PubMed: 19357407]

Wellen KE, Hotamisligil GS. Inflammation, stress, and diabetes. The Journal of clinical investigation. 2005; 115:1111–1119. [PubMed: 15864338]

Weyer C, Bogardus C, Mott DM, Pratley RE. The natural history of insulin secretory dysfunction and insulin resistance in the pathogenesis of type 2 diabetes mellitus. The Journal of clinical investigation. 1999; 104:787–794. [PubMed: 10491414]

White CL, Whittington A, Barnes MJ, Wang Z, Bray GA, Morrison CD. HF diets increase hypothalamic PTP1B and induce leptin resistance through both leptin-dependent and -independent mechanisms. Am J Physiol Endocrinol Metab. 2009; 296:E291–299. [PubMed: 19017730]

White CL, Whittington A, Barnes MJ, Wang ZQ, Bray G, Morrison CD. HF diets increase hypothalamic PTP1B and induce leptin resistance through both leptin-dependent and independent mechanisms. Am J Physiol Endocrinol Metab. 2008

Williams KW, Elmquist JK. From neuroanatomy to behavior: central integration of peripheral signals regulating feeding behavior. Nat Neurosci. 2012; 15:1350–1355. [PubMed: 23007190]

Williams KW, Margatho LO, Lee CE, Choi M, Lee S, Scott MM, Elias CF, Elmquist JK. Segregation of acute leptin and insulin effects in distinct populations of arcuate proopiomelanocortin neurons. J Neurosci. 2010; 30:2472–2479. [PubMed: 20164331]

Williams KW, Scott MM, Elmquist JK. Modulation of the central melanocortin system by leptin, insulin, and serotonin: co-ordinated actions in a dispersed neuronal network. Eur J Pharmacol. 2011; 660:2–12. [PubMed: 21211525]

Wu J, Bostrom P, Sparks LM, Ye L, Choi JH, Giang AH, Khandekar M, Virtanen KA, Nuutila P, Schaart G, et al. Beige adipocytes are a distinct type of thermogenic fat cell in mouse and human. Cell. 2012; 150:366–376. [PubMed: 22796012]

Xu C, Bailly-Maitre B, Reed JC. Endoplasmic reticulum stress: cell life and death decisions. The Journal of clinical investigation. 2005; 115:2656–2664. [PubMed: 16200199]

Yeo GS, Heisler LK. Unraveling the brain regulation of appetite: lessons from genetics. Nat Neurosci. 2012; 15:1343–1349. [PubMed: 23007189]

Yoshimura A, Naka T, Kubo M. SOCS proteins, cytokine signalling and immune regulation. Nat Rev Immunol. 2007; 7:454–465. [PubMed: 17525754]

Zabolotny JM, Bence-Hanulec KK, Stricker-Krongrad A, Haj F, Wang Y, Minokoshi Y, Kim YB, Elmquist JK, Tartaglia LA, Kahn BB, et al. PTP1B regulates leptin signal transduction in vivo. Dev Cell. 2002; 2:489–495. [PubMed: 11970898]

Zabolotny JM, Kim YB, Welsh LA, Kershaw EE, Neel BG, Kahn BB. Protein-tyrosine phosphatase 1B expression is induced by inflammation in vivo. J Biol Chem. 2008; 283:14230–14241. [PubMed: 18281274]

Zhang X, Zhang G, Zhang H, Karin M, Bai H, Cai D. Hypothalamic IKKbeta/NF-kappaB and ER stress link overnutrition to energy imbalance and obesity. Cell. 2008; 135:61–73. [PubMed: 18854155]

Article Highlights

1. Xbp1s in Pomc neurons protects against ER stress induced leptin/insulin resistance
2. Xbp1s in Pomc neurons improves glucose levels and hepatic insulin sensitivity
3. Pomc-specific xbp1s protects against high-fat diet induced obesity
4. *Pomc*-specific *xbp1s* regulates the UPR^{ER} in the liver

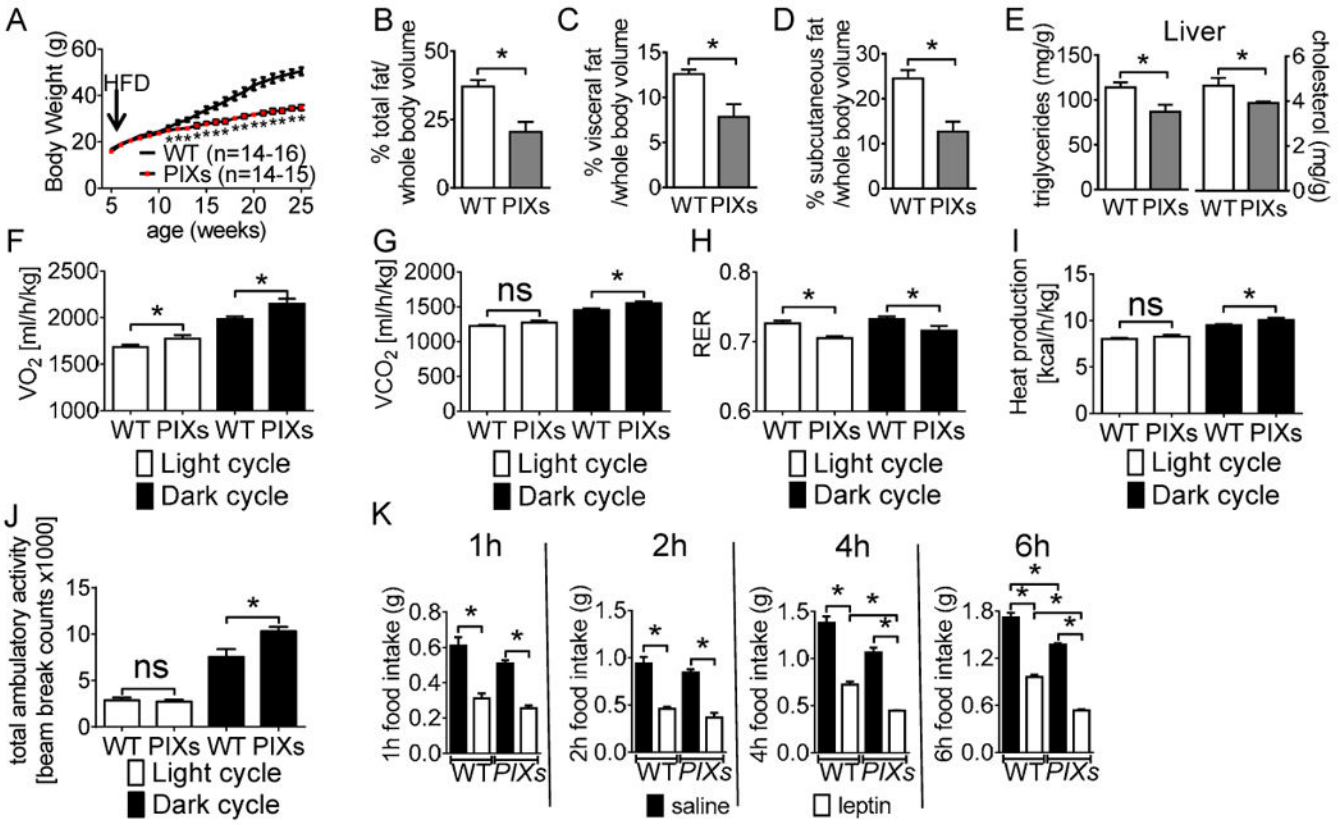

Figure 1.

Body weight and metabolic assessment of male WT and PIXs mice on HFD. Body weight curve of (A) male PIXs mice (*p<0.05). Body fat composition: whole body volume (B), visceral (C), and subcutaneous (D). Male PIXs mice display (E) increased hepatic triglyceride and cholesterol, (F) Increased VO_2, (G) increased VCO_2, (H) decreased RER (I) increased heat production, and (J) increased ambulatory activity. Error bars indicate SEM. (K) Leptin induced hypophagia was observed at 1, 2, 4, and 6 after refeeding. *PIXs* mice exhibited increased hypophagia in response to pharmacological administration of leptin at 4 and 6 hours after refeeding. (n=10 per group; *p<0.05). (Note: mice used in (E-I) were age-matched male littermates (8 weeks of age), and had comparable body weight and lean mass. (for F-J, n=14-16 per group; *p<0.05).

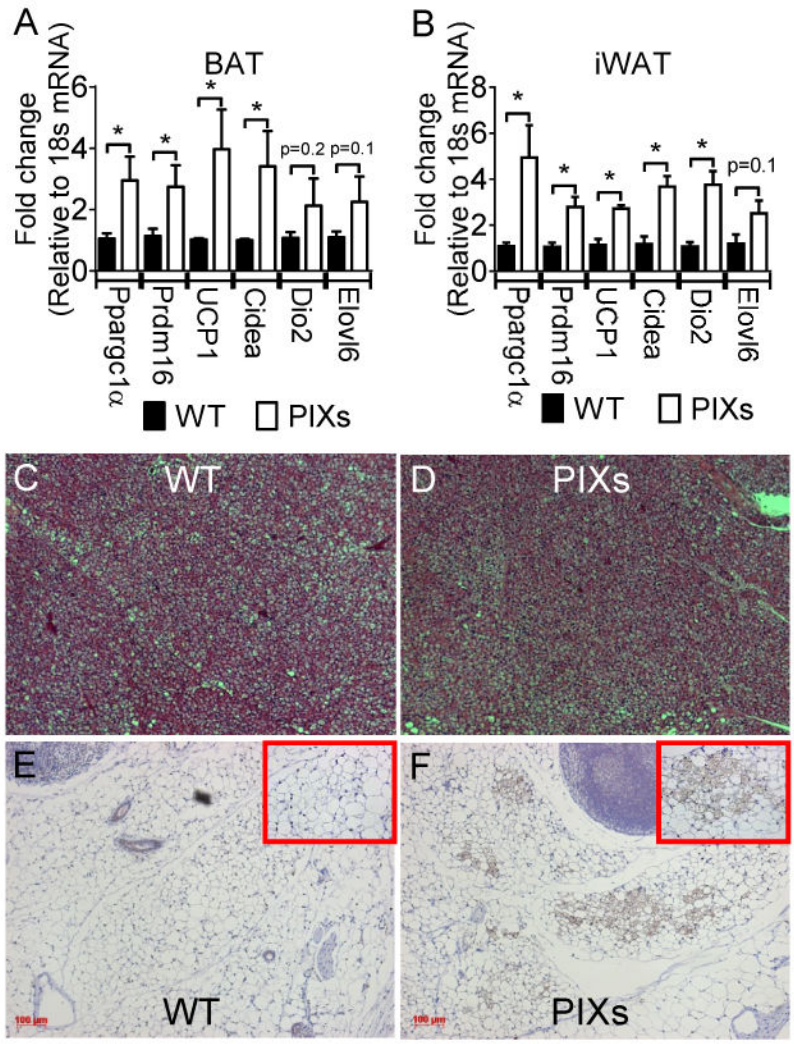

Figure 2.

PIXs mice express increased thermogenic markers in BAT and iWAT. Weight matched *PIXs* mice were fed HFD DOX enriched diet for 2 weeks. qPCR was performed to examine the relative expression Ppargc1α, Prdm16, UCP1, Cidea, Dio2, and Elovl6 which are known genes associated with heat production in (A) BAT and (B) iWAT. *, $p < 0.05$. Brown adipose tissue (BAT) from (C) WT and (D) PIXs mice was imaged by light microscopy after hematoxylin-eosin staining. Inguinal white adipose tissue from (E) WT and (F) PIXs mice was imaged by light microscopy after UCP-1 immunohistochemistry. Bars, 100μm. (note C and D are the same scale as E and F).

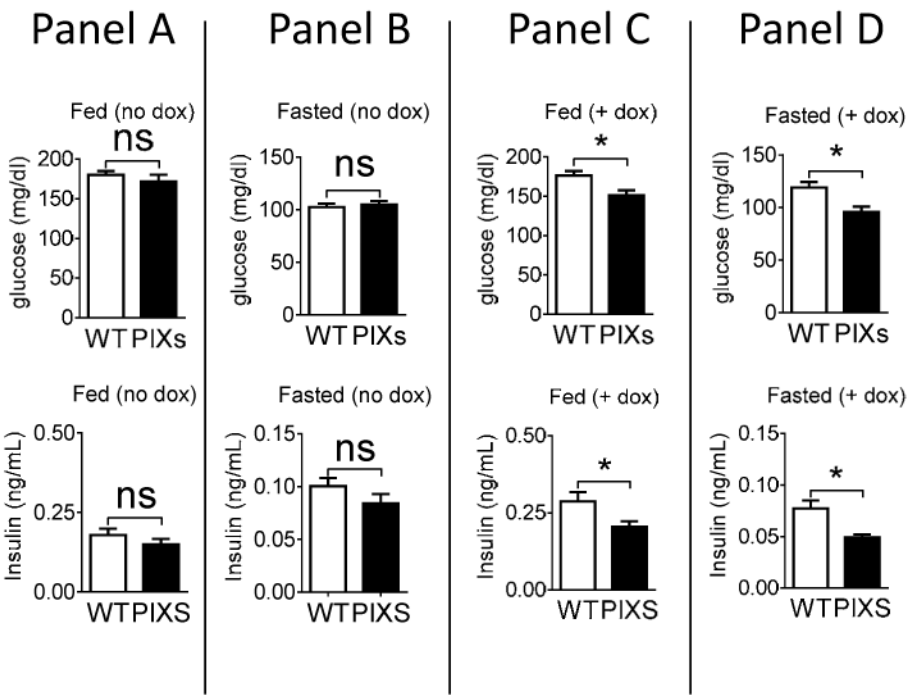

Figure 3.

Blood glucose and insulin levels of male WT and PIXs mice on chow diet. Blood glucose and insulin levels were measured from WT and PIXs mice fed chow diet without dox (Panel A), fed on a chow diet without dox then fasted overnight (Panel B), fed a chow diet with dox for 1 week (Panel C), and fed chow diet with dox for 1 week then fasted overnight (Panel D). Blood glucose and insulin levels were decreased in mice fed or fasted after 1 week on a chow diet with dox (n=10-15 per group; $^{*}p<0.05$).

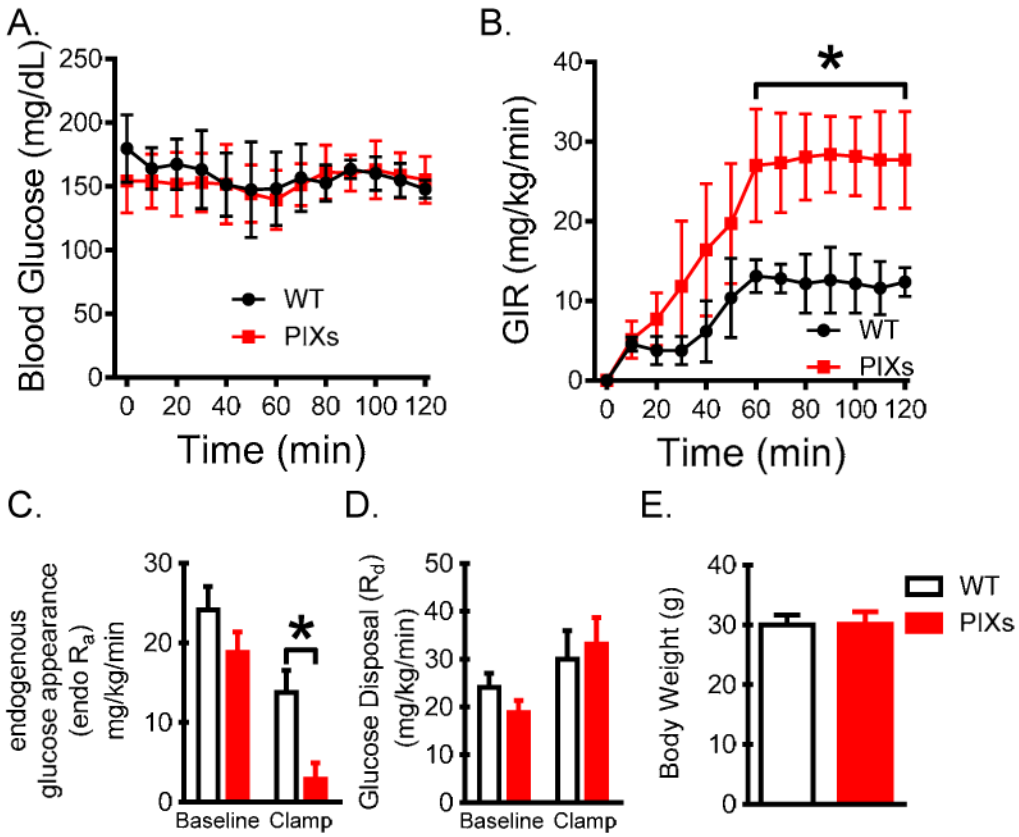

Figure 4.

Improved glucoregulation in mice which constitutively express Xbp1s in Pomc neurons. (A) Basal and clamp blood glucose levels during the hyperinsulinemic-euglycemic experiment. (B) Exogenous glucose infusion rate (GIR) needed to clamp blood glucose. (C and D) Endogenous rates of glucose appearance (endo Ra) and disappearance (Rd) were determined using a constant infusion of [3-3H]glucose and Steele's steady-state calculations. (E) Body weight of PIXs mice on day of experiment. (n=7)

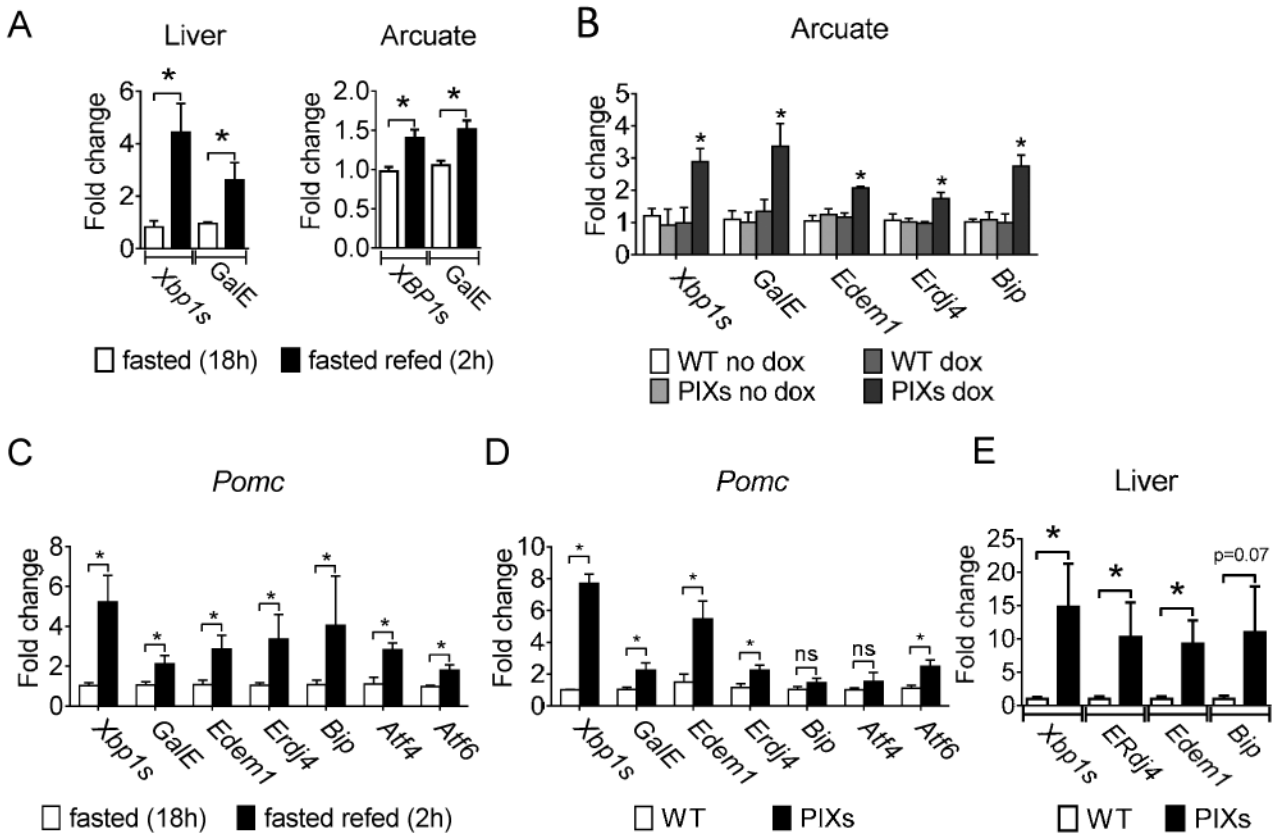

Figure 5.

Regulation of *Xbp1s and GalE* in the arcuate nucleus and the liver. (A) Relative mRNA expression of *Xbp1s* and *GalE* in the liver and the arcuate nucleus of mice fasted (18h) and mice re-fed (2h) after fasting (18h). (B) Relative mRNA expression of *Xbp1s* as well as *GalE, Edem1, Erdj4*, and *Bip*, which are which are known Xbp1s target genes, in the arcuate nucleus from *PIXs* and *WT* mice fed either non-Dox or Dox containing diet. (C-D) Relative mRNA expression *of Xbp1s, GalE, Edem1, Erdj4, Bip, Atf4*, and *Atf6* in FACS-Pomc neurons. (C) Data represents from WT mice fasted (18h) and WT mice re-fed (2h) after fasting (18h). (D) Data represents *PIXs* and *WT* mice chronically fed Dox containing diet. (E) qPCR was performed on mice chronically fed HF-Dox diet to examine the relative expression XBP1s as well as erdj4, erdeml, chop, and bip which are which are known Xbp1s target genes in (L) liver. $^{*}P < 0.05$ compared with control. A-E. Fold change relative to 18S mRNA; Error bars indicate SEM.

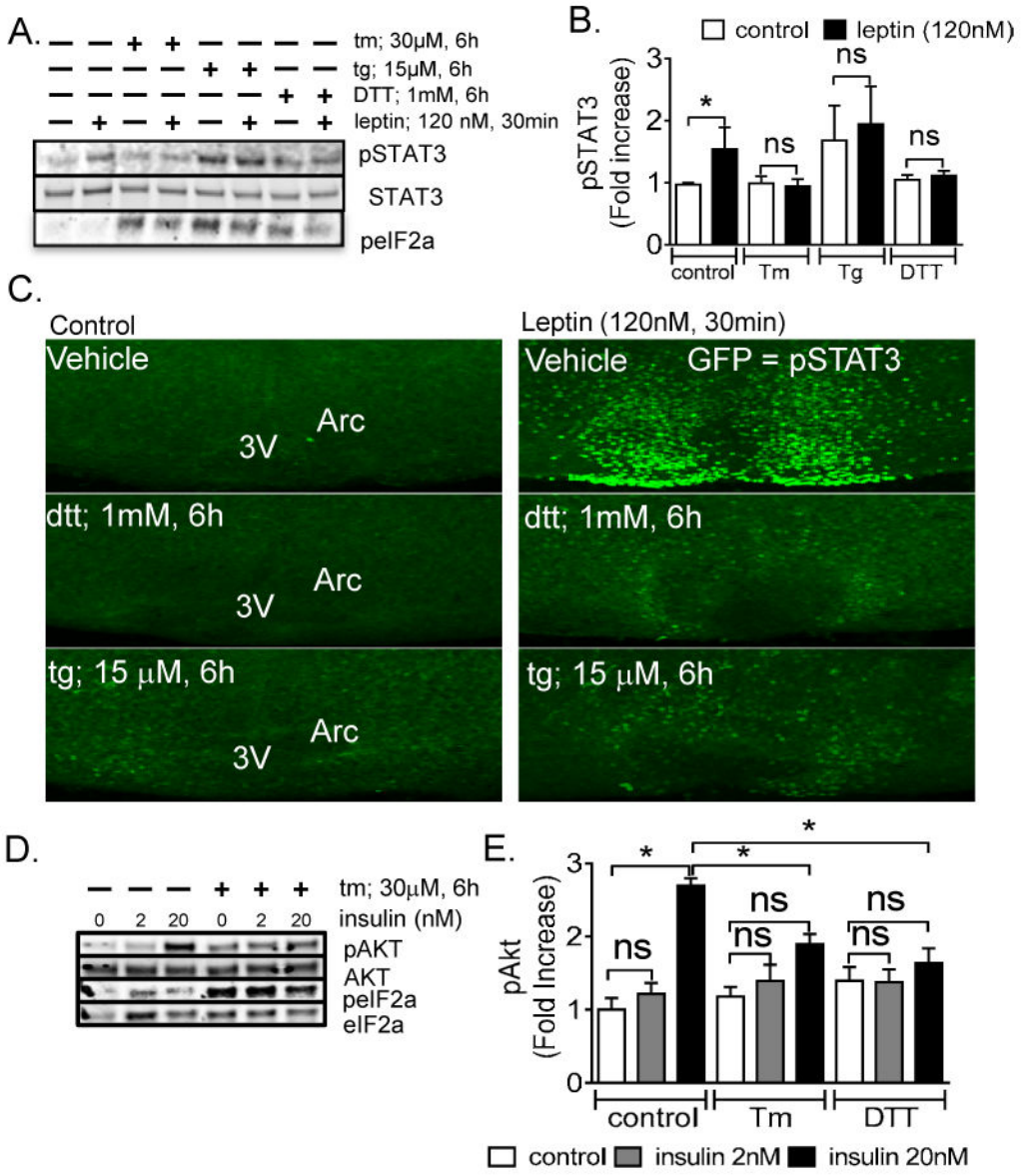

Figure 6.

ER stress blunts the leptin and insulin activity in the Arcuate nucleus (A) Blots represent changes in the protein levels for leptin-induced phospho-STAT3 and phospho-eif2α in response to ER stress. (B) Quantitative densitometry for protein expression of leptin-induced pSTAT3 in control and ER stress activators. (C) ER stress blunts leptin-induced pSTAT3 immunoreactivity in the arcuate nucleus of the hypothalamus. ($^{*}P < 0.05$, values are means ±SEM from 3-6 independent experiments, error bars indicate SEM) (D) Blots represent changes in the protein levels for insulin-induced phospho-AKT and phospho-eif2α in response to ER stress. (E) Quantitative densitometry for the protein expression of insulin-induced pAKT.

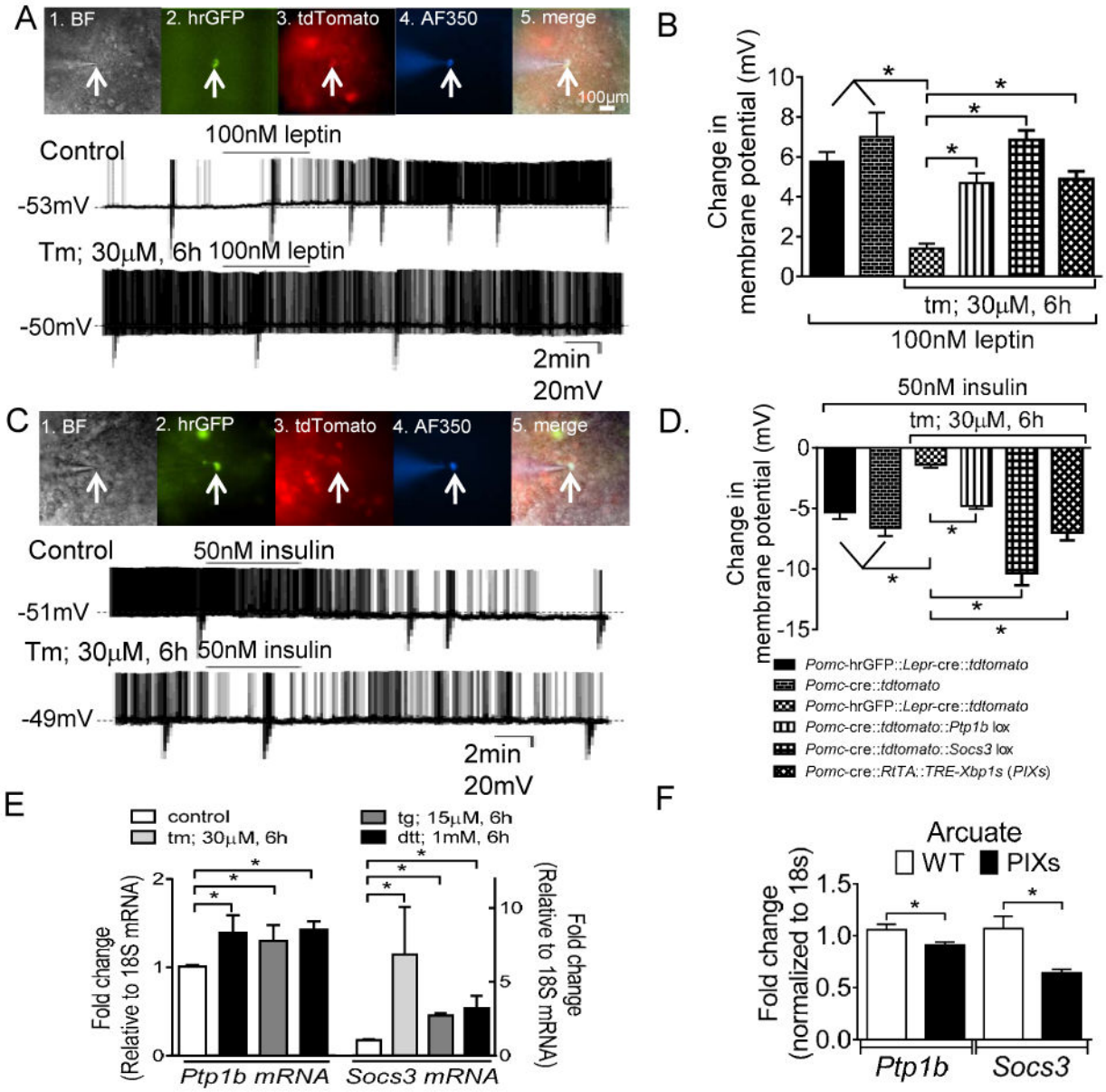

Figure 7.

ER stress blunts the leptin-induced activation and the insulin-induced inhibition of *Pomc* neurons. (A) 1. Brightfield illumination of *Pomc-hrGFP::Lepr-cre::tdtomato* neuron from *PLT* mice. 2. and 3. The same neuron under FITC (hrGFP) and Alexafluor 594 (*tdtomato*) illumination. 4. Complete dialysis of Alexa Fluor 350 from the intracellular pipette. 5. Merge image illustrates colocalization of hr-GFP, *tdtomato*, and Alexa Fluor 350 indicative of a *Pomc* neuron which expresses *Leprs*. Control (above). Electrophysiological study demonstrates a *Pomc*-hrGFP::*Lepr*-cre::*tdtomato* (green/red) neuron that depolarized in response to leptin. Below demonstrates a current clamp recording of a separate *Pomc*-hrGFP::*Lepr*-cre::*tdtomato* (green/red) neuron in which ER stress blunted the leptin induced depolarization. (B) Histogram demonstrating that multiple activators of ER stress blunted the leptin-induced activation of *Pomc* neurons (n= 8-15 per group). Deletion of either *Ptp1b*

or *Socs3* restores the leptin-induced excitation of arcuate Pomc neurons after ER stress induction. Similarly, constitutive expression of *Xbp1s* in Pomc neurons restores the leptin-induced excitation of arcuate Pomc neurons after ER stress induction. $^{*}P < 0.05$. Error bars indicate SEM. (C) 1. Brightfield illumination of *Pomc*-hrGFP neuron from *PLT* mice. 2. and 3. The same neuron under FITC (hrGFP) and Alexafluor 594 (*tdtomato*) illumination. 4. Complete dialysis of Alexa Fluor 350 from the intracellular pipette. 5. Merge illustrates colocalization of hr-GFP and Alexa Fluor 350 indicative of a *Pomc* neuron which does not expresses *Lepr*s. Control (above): Electrophysiological study demonstrates a *Pomc*-hrGFP (green) neuron is hyperpolarized in response to insulin. Below: A separate *Pomc*-hrGFP (green) neuron in which ER stress blunts the insulin induced hyperpolarization. (D) Histogram illustrating that chemical activation of ER stress blunts the insulin-induced inhibition of arcuate *Pomc* neurons (n= 8-18 per group). Deletion of either *Ptp1b* or *Socs3* restores the insulin-induced inhibition of arcuate Pomc neurons after ER stress induction. $^{*}P < 0.05$, Error bars indicate SEM. (E) Relative mRNA expression of *Socs3* and *Ptp1b* in organotypic slices following pretreatment with ER stress activators. (F) Relative mRNA of *Ptp1b* and *Socs3* in the arcuate nucleus from *PIXs* and *WT* mice fed HFD-Dox. ($^{*}P < 0.05$, values are means ±SEM from 3-6 independent experiments, error bars indicate SEM)